J. Eng. Technol. Sci., Vol. 54, No. 6, 2022, 220604

# Influence of the Process Parameters on the Microhardness and the Wear Resistance of Friction Stir Processed H65 Copper Alloy

**Xiaole Ge[1,2], Igor Kolupaev[1,*], Weiwei Song[2], Di Jiang[1,2], Jiafei Pu[2], Hongfeng Wang[2] & Yuan Chu[2]**

[1]Department of Materials Science, National Technical University «Kharkiv Polytechnic Institute», Kharkiv, 61002, Ukraine
[2]College of Mechanical and Electrical Engineering, Huangshan University, Huangshan, Anhui, 245041, China
*E-mail: igor2018kolupaev@gmail.com

**Highlights:**

- A larger-size surface of H65 copper alloy was modified by using friction stir processing (FSP).
- The influence of the FSP process parameters on the microstructure, the microhardness and the wear resistance of the modified H65 copper alloy was explored.
- The wear mechanism of the modified H65 copper alloy was revealed.

**Abstract.** Friction stir processing (FSP) was used to modify a larger-size surface of H65 copper alloy. The influence of the traverse speed and the rotation speed on the microstructure, the microhardness and the wear resistance of the modified surface were analyzed. The wear mechanism of the modified H65 copper alloy was revealed. The results indicate that the grain size was greatly refined after FSP compared with the parent metal and that the grain size increased with the increment of the rotation speed. The average microhardness of the modified surface was higher than that of the parent metal. The average microhardness had a highest value of 174.13 HV when the traverse speed was 200 mm/min and the rotation speed was 200 rpm, i.e., 21% higher than that of the parent metal. The average microhardness decreased with the increase of the rotation speed. When the traverse speed was 200 mm/min and the rotation speed was 600 rpm, the average friction coefficient of the modified surface was the smallest (0.3213), which was lower than that of the parent metal (0.3810). The wear mechanism of the H65 copper alloy modified by FSP was mainly adhesive wear accompanied by local abrasive wear.

**Keywords**: *friction stir processing; H65 copper alloy; microhardness; microstructure; wear resistance.*

Received January 13th, 2022, 1st Revision August 5th, 2022, 2nd Revision October 14th, 2022, Accepted for publication October 24th, 2022.

DOI: 10.5614/j.eng.technol.sci.2022.54.6.4

## 1 Introduction

Copper and its alloys are the third most commonly used materials in industrial production, second only to steel/iron and aluminum alloys [1]. Copper alloys are widely used in the fields of electric power, shipbuilding, mechanical equipment, aerospace and others because of their high strength, excellent corrosion resistance and good processing properties [2-3]. However, copper alloys have low hardness and poor wear resistance, which limits their application range [4]. Some copper alloy parts that have direct contact and relative movement often fail due to low surface hardness and poor wear resistance, which reduces their service life to a certain extent [5]. In order to prolong the service life of copper alloy parts, it is necessary to explore reasonable and economical processing methods to improve their surface properties. Commonly used metal surface treatment methods are laser cladding, electroplating, plasma spraying, etc. [6-7]. These methods can obtain better surface properties, but the treatment process is complex, the cost is high, and pollution is prone to occur.

Treating the metal surface in an economical and environmentally friendly way to obtain ideal surface performance is a constant pursuit in industrial production [8-9]. Fortunately, Mishra, *et al*. [10] developed the friction stir processing (FSP) technique based on friction stir welding to achieve this goal. The basic principle of FSP is to utilize the stirring action of the tool to produce local plastic deformation of the material in the processing area and at the same time generate a large amount of heat, thereby changing the material properties of the processing area [11]. FSP is widely used in the surface modification of aluminum alloys, magnesium alloys, copper alloys and steel because of its simple processing technology, its low cost, and the absence of pollution to the environment [12].

Many researchers have studied the FSP properties of copper and copper alloys. Song, *et al*. [13-14] modified a H62 copper alloy surface by FSP and analyzed the corrosion resistance and the wear resistance of the processed surface. They found that the corrosion resistance and wear resistance after FSP were greatly improved compared with the parent metal. Heidarpour, *et al*. [15] carried out FSP on a Cu-$TiO_2$ surface and explored the influence of pass number on the microstructure, corrosion resistance, and mechanical properties of the processed surface. Sarmadi, *et al*. [16] studied the wear performance of copper-graphite composites after FSP, focusing on the analysis of the effect of graphene content on the friction coefficient and wear loss.

Furthermore, Cartigueyen & Mahadevan [17] studied the influence of the rotation speed of the tool in the forming of a pure copper plate in FSP and discussed the relationship between the heat input and the mechanical properties of the processed surface. In FSP studies, the tool path is currently only a single straight

line and few studies have been carried out on larger-size surfaces. However, in actual engineering applications, the modification of larger-size surfaces has more application potential and value. Therefore, it is necessary to study larger-size surface modification of copper and copper alloys by FSP.

In this paper, the H65 copper alloy was taken as the research object. The first aim was to realize larger-size surface modification of the H65 copper alloy by FSP. The second aim was to explore the influence of the FSP process parameters on the microstructure, the microhardness and the wear resistance of the modified surface. The research content of this work provides a reference for larger-size surface modification of copper alloys.

## 2 Experimental Procedure

A rolled H65 copper alloy plate with a thickness of 10 mm was used to carry out the experiments with an FSP machine. The length and width of the copper alloy plate were 200 mm and 100 mm, respectively. Table 1 gives the chemical composition of the H65 copper alloy plate.

**Table 1** Summary of chemical composition (mass fraction, %).

| Elements | Cu | Pb | P | Fe | Sb | Bi | Zn | Impurities |
|---|---|---|---|---|---|---|---|---|
| Content | 63.5-68 | 0.03 | 0.01 | 0.1 | 0.005 | 0.005 | Balance | 0.3 |

The tool used in the FSP experiments are shown in Figure 1. The shoulder diameter of the tool was 20 mm and the material of the tool was H13. The tilt angle of the tool was set to 0° in all FSP experiments.

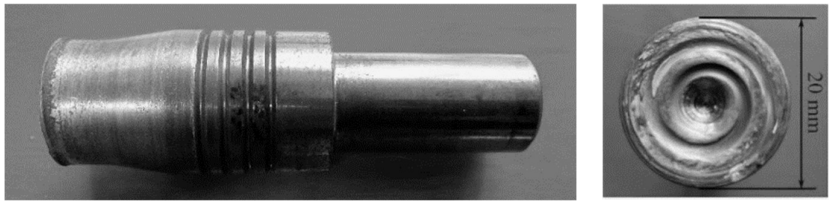


**Figure 1** The shape of tool.

Previous studies have shown that the traverse speed and the rotation speed have an important impact on the quality of the modified layer [18-19]. To explore the changes of the microstructure, microhardness and wear resistance of the H65 copper alloy at different traverse speeds and rotation speeds, nine groups of experiments were set up, as listed in Table 2. The machining depth of the tool was set to 0.5 mm in all FSP experiments. For ease of description, the traverse speed and the rotation speed are denoted by the abbreviations T and R.

**Table 2** Parameter settings in FSP experiments.

| Sample No. | Traverse speed (mm/min) | Rotation speed (rpm) |
|---|---|---|
| 1 | 100 | 200 |
| 2 | 100 | 400 |
| 3 | 100 | 600 |
| 4 | 200 | 200 |
| 5 | 200 | 400 |
| 6 | 200 | 600 |
| 7 | 300 | 200 |
| 8 | 300 | 400 |
| 9 | 300 | 600 |

In order to realize FSP on a larger-size surface, the tool moved along the processing path 1-2-3-4-5-6-7-8-9-10-11-12-13-14-15-3-16 on the surface to be processed, as shown in Figure 2. The microstructure test samples, the microhardness test samples and the wear resistance test samples were extracted from the FSP zone by using a wire cutting machine. The positions of the different types of test samples are shown in Figure 2.

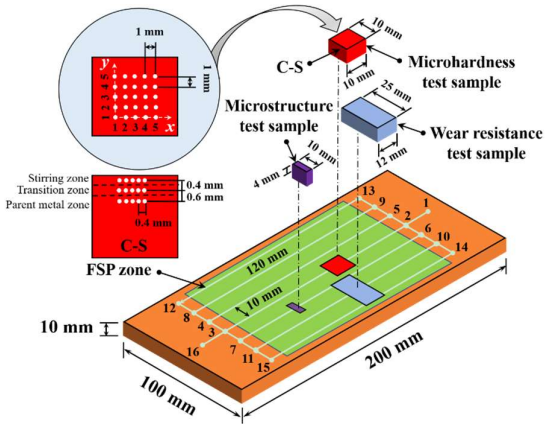


**Figure 2** Schematic diagram of processing path and sample preparation.

The microstructure test samples were observed with a YM520R-type microscope after the following three processing procedures. Firstly, metallographic sandpaper (320 #, 600 # and 1000 #) was used to grind the processed surface of the microstructure test samples until the surface was smooth. Secondly, the ground microstructure test samples were electropolished with an electrolytic polishing machine to remove surface scratches. The corrosion voltage, the corrosion current and the corrosion time were set to 50 V, 4.5 A and 12 s, respectively. Finally, a mixed solution of ferric chloride (2.5 g), hydrogen chloride (5 ml), methanol (50 ml) and water (50 ml) was adopted to corrode the

electropolished surface with a corrosion time of about 10 s. Due to the different physical and chemical properties between grains, between grains and grain boundaries, and between phases in the copper alloy, the corrosion rates of different microstructures in electrolyte solution are different, resulting in different refractive indexes under the microscope, by which different grains can be distinguished. The three-circle intercept point method (500 mm), i.e., using three concentric equidistant circles with a total circumference of 500 mm, was adopted to measure the grain size using the Metallographic Image Analysis Software provided by Jinan Times Testing Machine Technology Co., Ltd.

The processed surfaces of the microhardness test samples were first ground to smooth with metallographic sandpaper (320 #, 600 # and 1000 #), and then polished with an MDS600-type metallographic polishing machine. Subsequently, an HV-1000-type microhardness tester was used to test the microhardness of the polished surface. The test load was 1.0 kg and the loading time was 10 s. In order to reasonably characterize the microhardness of the processed surface, twenty-five points were tested for each sample. The processed surfaces of the wear resistance test samples were first polished to smooth with metallographic sandpaper (320 #, 600 # and 1000 #). Afterwards, friction and wear tests were performed using an HT-1000-type friction and wear tester. The grinding material was Cr, the friction radius was 2 mm, the load was 650 N, and the test time was 5 min. The wear surface morphologies were observed using an S-3400N-type scanning electron microscope (SEM). A three-dimensional superdepth digital microscope was used to measure the three-dimensional shape and the surface roughness of the processed surfaces.

## 3 Results and Discussion

### 3.1 Macro Morphology of the Processed Surfaces

Figure 3 shows the macro surface morphologies under different FSP conditions. It can be seen from Figure 3 that the processed surfaces were well-formed under different process parameters and that the processed surfaces were relatively flat, without obvious surface defects, which indicates that it is feasible to modify a larger-size surface of the H65 copper alloy by FSP. Figure 3 also shows that the greater the traverse speed, the rougher the tool lines and the greater the surface roughness (Sa). The higher the rotation speed, the smaller the tool lines and the lower the surface roughness. The processed surface roughness of Sample 7 was the highest (44.14 μm) and the processed surface roughness of Sample 3 was the lowest (25.03 μm), both higher than that of the parent metal (22.13 μm). It should be noted that the FSP is only one of the key processes of surface modification, and the rough surface formed by tool lines and processing burrs has to be subjected to subsequent surface treatment to meet the actual use requirements.

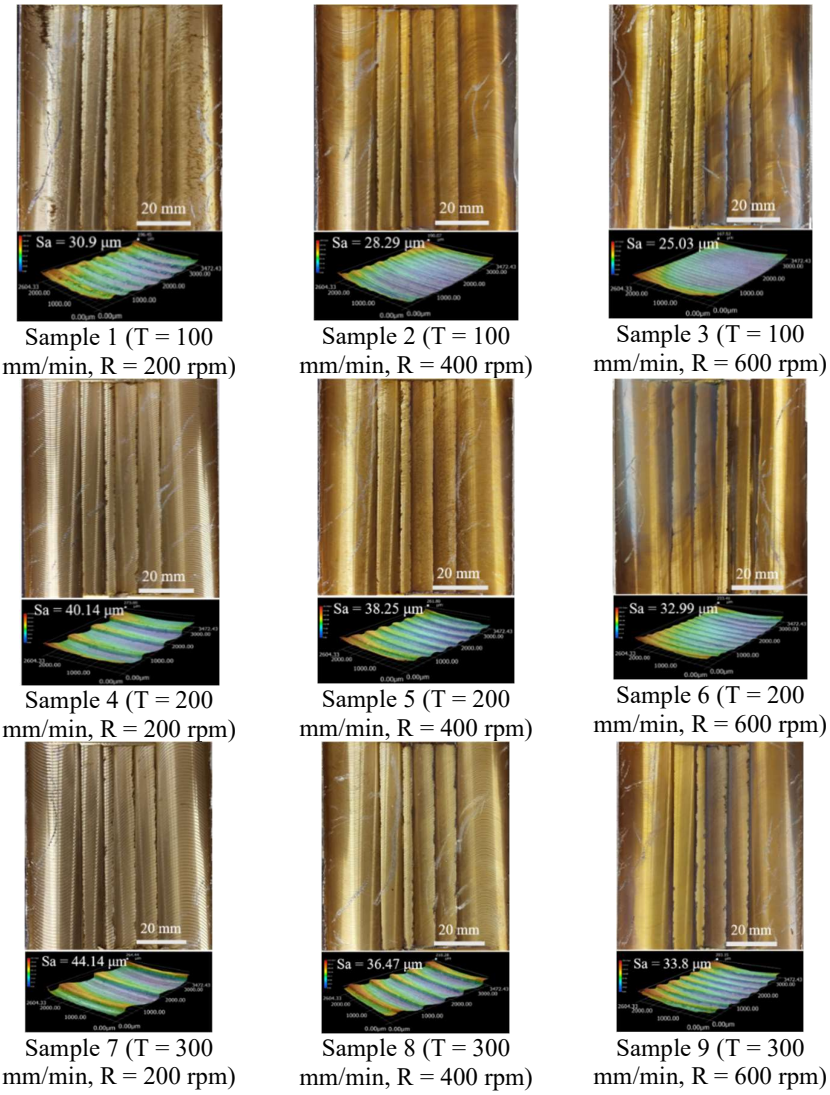


**Figure 3** Macro surface morphologies under different process parameters.

## 3.2 Microstructure of the processed surface

Figure 4 shows the microstructure of the parent metal and the processed surface under different process parameters.

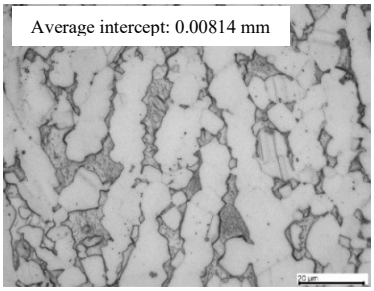


Parent metal

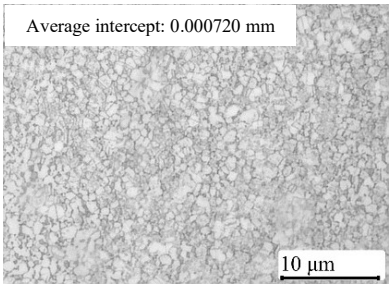


Sample 1 (T = 100 mm/min, R = 200 rpm)

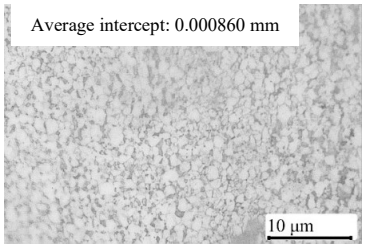


Sample 2 (T = 100 mm/min, R = 400 rpm)

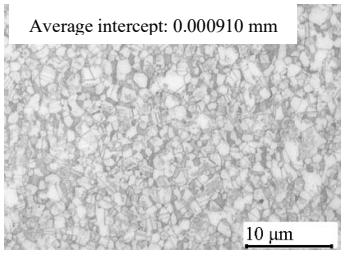


Sample 3 (T = 100 mm/min, R = 600 rpm)

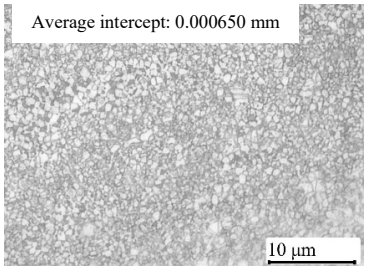


Sample 4 (T = 200 mm/min, R = 200 rpm)

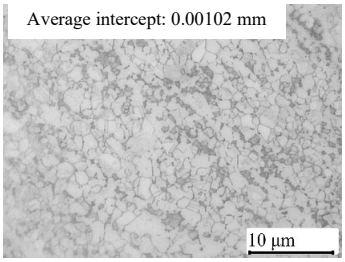


Sample 5 (T = 200 mm/min, R = 400 rpm)

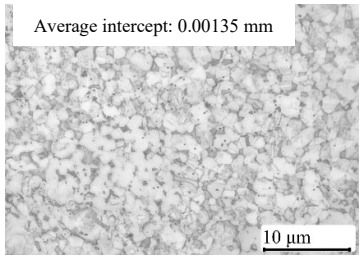


Sample 6 (T = 200 mm/min, R = 600 rpm)

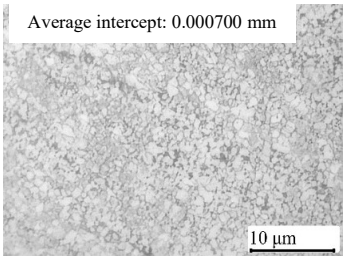


Sample 7 (T = 300 mm/min, R = 200 rpm)

Average intercept: 0.000960 mm

Average intercept: 0.00111 mm

**Figure 4** Microstructure of parent metal and processed surface under different process parameters.

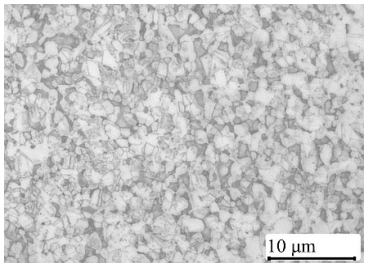


Sample 8 (T = 300 mm/min, R = 400 rpm)

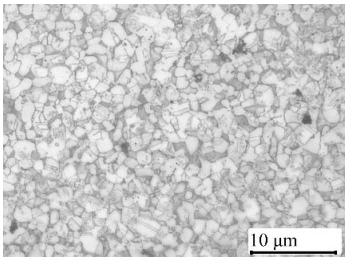


Sample 9 (T = 300 mm/min, R = 600 rpm)

**Figure 4 Continued.** Microstructure of parent metal and processed surface under different process parameters.

It is evident from Figure 4 that the average intercept of grains on the processed surface was greatly reduced compared with the parent metal, which demonstrates that FSP can effectively refine grains. This is consistent with the research reported in [20]. The reason for the grain refinement is mainly the intense plastic deformation of the material caused by the strong stirring effect of the tool during the FSP process [21]. In addition, the grain refinement is also related to the degree of dynamic recrystallization generated at high temperature [22]. Reference [23] has shown that the friction heat and the plastic deformation during FSP are mainly related to the rotation speed of the tool.

The higher the rotation speed, the more friction heat and the greater the plastic deformation. It can be seen from Figure 4 that the average intercept of grains increased with the increment of the rotation speed at the same traverse speed. This is mainly because more heat is generated in the FSP zone under a higher rotation speed, resulting in the grains growing at higher temperature [24]. On the whole, the average intercept of grains of Sample 4 was the lowest (0.000650 mm), which indicates that the microhardness may be highest when the traverse speed is 200 mm/min and the rotation speed is 200 rpm.

Figure 5 shows the cross-sectional microstructure of Sample 4. The cross-sectional microstructure can be divided into three zones: stirring zone, transition zone, and parent metal zone. The grain size in the stirring zone was uniform and the average intercept of the grains was the lowest. The grains in the parent metal zone were coarse and strip-shaped and the average intercept of grains was the highest. The grain size of the transition zone was between that of the stirring zone and the parent metal zone. The depth of the stirring zone was about 315 μm and the depth of the transition zone was about 390 μm.

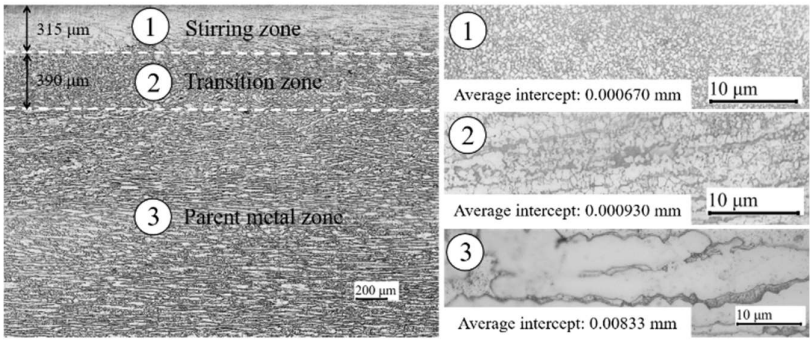


**Figure 5** Cross-sectional microstructure of Sample 4.

### 3.3 Microhardness of the Processed Surface

In order to reasonably evaluate the microhardness of the processed surface, twenty-five microhardness values were tested for each sample according to the method illustrated in Figure 2 and the average microhardness was calculated as shown in Figure 6.

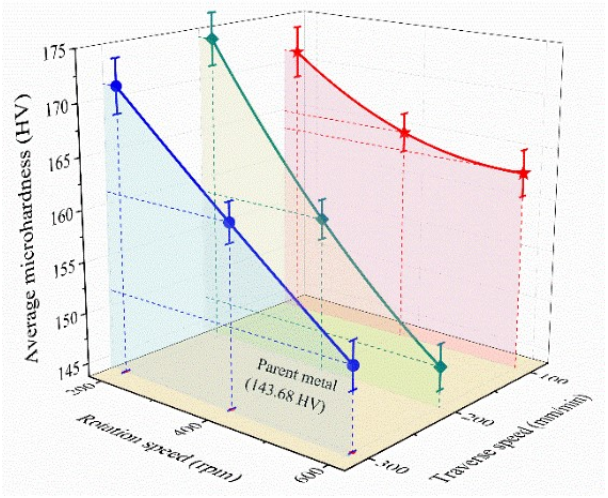


**Figure 6** Average microhardness of parent metal and processed surface under different process parameters.

It is obvious from Figure 6 that the average microhardness under different process parameters was higher than that of the parent metal. When the traverse speed was 200 mm/min and the rotation speed was 200 rpm, the highest average

microhardness of the processed surface was 174.13 HV, i.e., 30.45 HV higher than that of the parent metal at 143.68 HV. When the traverse speed was 200 mm/min and the rotation speed was 600 rpm, the average microhardness of the processed surface was the lowest, at 147.56 HV, i.e., still higher than that of the parent metal. Microhardness is mainly affected by the grain size, heat production, volume fraction, and distribution of the second phase, the quench hardening and so on [17,25]. The Hall-Petch relationship indicates that a smaller grain size helps to obtain higher microhardness [26-28]. It is evident from the microstructure analysis that the grain size after FSP was greatly reduced compared with the parent metal, which is consistent with the improvement of the microhardness. Figure 6 also shows that the microhardness of the processed surface decreased with the increase of the rotation speed at the same traverse speed. This is mainly because more heat is generated by FSP at a higher rotation speed and the fine grains broken by the tool grow more easily under high temperature condition, resulting in a lower microhardness. This finding is consistent with the results of [17,29]. From another perspective, there is no exact relationship between the traverse speed and the average microhardness under the same rotation speed.

To understand the microhardness distribution at the cross-section of the processed surface, the cross-sectional microhardness of Sample 4 was tested in the stirring zone, the transition zone, and the parent metal zone according to the schematic (C-S) illustrated in Figure 2. The average microhardness was calculated as shown in Figure 7.

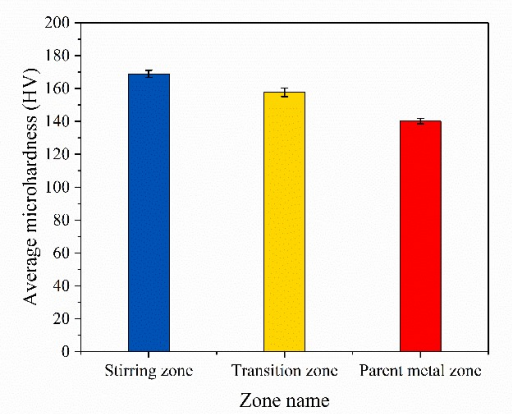


**Figure 7** Average microhardness in different zones of the cross-section of the processed surface.

Figure 7 shows that the microhardness of the stirring zone was the highest, followed by the transition zone, while the microhardness of the parent metal zone was the lowest. The average microhardness of the stirring zone was 168.96 HV,

which is close to the microhardness of the processed surface. It can be inferred from Figure 5 and Figure 7 that the microhardness distribution in different zones at the cross-section of the processed surface is closely related to the corresponding microstructure, a smaller grain size contributes to a higher microhardness.

### 3.4 Wear Resistance of the Processed Surface

The friction coefficients of the parent metal and the processed surface under different process parameters are shown in Figure 8. It shows that the friction coefficients under different process parameters were different and only some process parameters had lower friction coefficients than the parent metal.

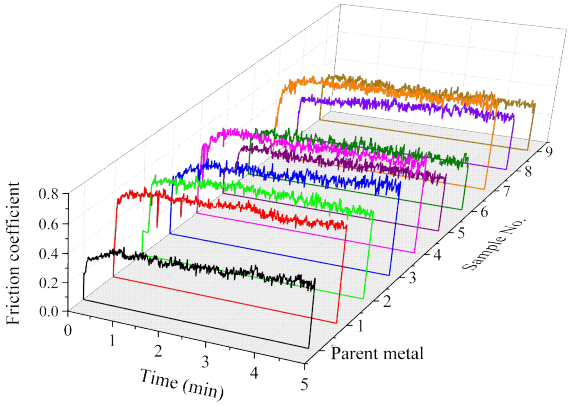


**Figure 8** Friction coefficients of the parent metal and the processed surface under different process parameters.

In order to further analyze the variation rule of friction coefficient under different process parameters, the average friction coefficient was calculated as shown in Figure 9. Figure 9 shows that the minimum average friction coefficient was 0.3213, when the traverse speed was 200 mm/min and the rotation speed was 600 rpm, i.e., lower than that of the parent metal (0.3810). When the traverse speed was 100 mm/min and the rotation speed was 200 rpm, the maximum average friction coefficient was 0.6156, i.e., higher than that of the parent metal. Furthermore, the average friction coefficient decreased with the increase of the rotation speed when the traverse speed remained unchanged, which is consistent with the change trend of the average microhardness. This phenomenon implies that there is no absolute negative correlation between friction coefficient and microhardness, and a comprehensive analysis needs to be carried out in combination with the actual situation. This view is also indicated in [30].

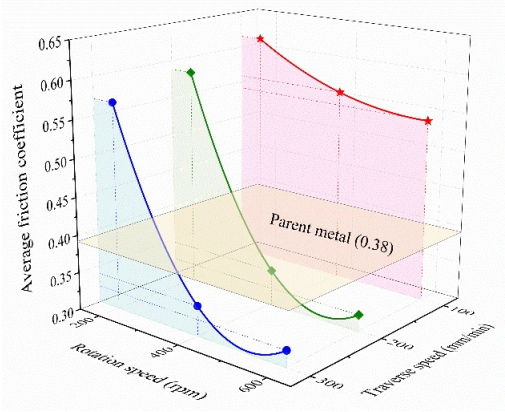


**Figure 9** Average friction coefficients of parent metal and processed surface under different process parameters.

The phenomenon that the higher the microhardness, the greater the friction coefficient may be caused by (i) larger residual stress produced in the processed surface during FSP, and (ii) enhanced brittleness of the processed surface due to high microhardness. In a sample with higher microhardness, microcracks tend to appear in the friction surface during the sliding process between the sample and the grinding ball. As the friction continues, the microcracks continue to expand to the surface and the depth direction [31], and the friction surface becomes uneven due to the continuous transfer and peeling of the material [32], resulting in a higher friction coefficient of the friction surface.

In order to clarify the wear mechanism of the H65 copper alloy, the morphologies of the wear surface were observed by SEM, as shown in Figure 10.

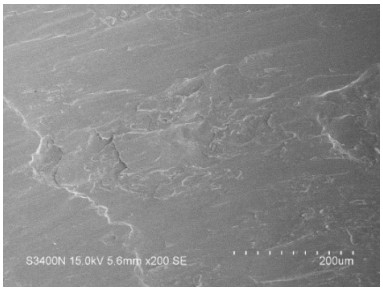


Parent metal

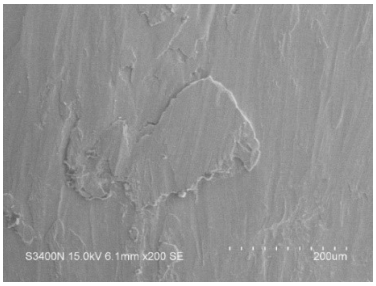


Sample 1 (T = 100 mm/min, R = 200 rpm)

**Figure 10** Wear surface morphologies of the parent metal and the processed surface under different process parameters.

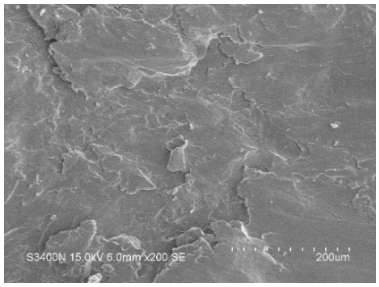


Sample 2 (T = 100 mm/min, R = 400 rpm)

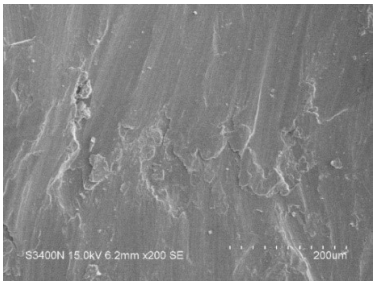


Sample 3 (T = 100 mm/min, R = 600 rpm)

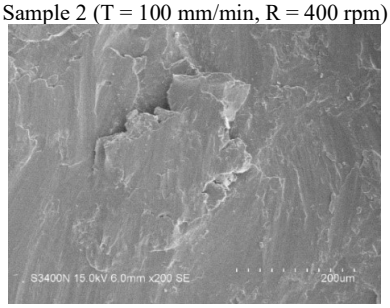


Sample 4 (T = 200 mm/min, R = 200 rpm)

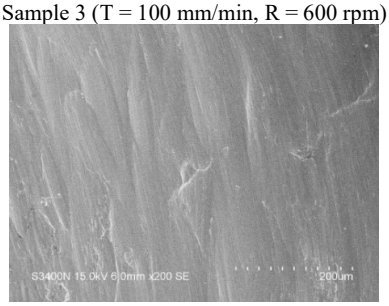


Sample 5 (T = 200 mm/min, R = 400 rpm)

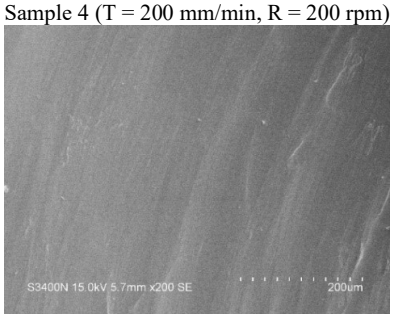


Sample 6 (T = 200 mm/min, R = 600 rpm)

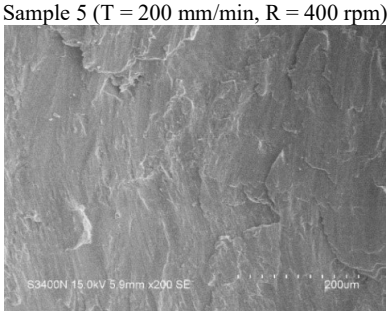


Sample 7 (T = 300 mm/min, R = 200 rpm)

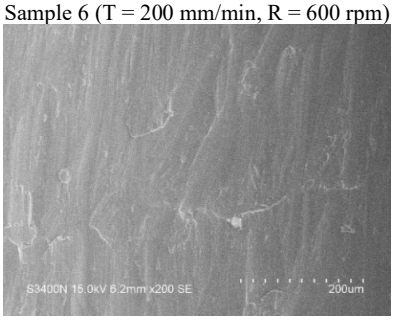


Sample 8 (T = 300 mm/min, R = 400 rpm)

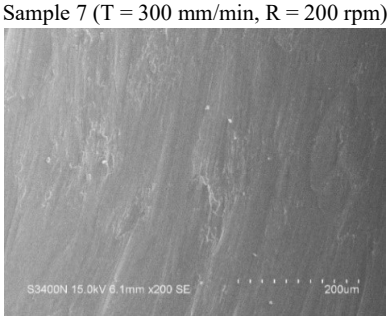


Sample 9 (T = 300 mm/min, R = 600 rpm)

**Figure 10 Continued.** Wear surface morphologies of the parent metal and the processed surface under different process parameters.

It can be seen from Figure 10 that there were certain material plastic flow traces on the wear surface. Some samples (such as Samples 1, 2, 3, 4, and 7) had an obvious tendency to cast off wear debris, which is a typical feature of adhesive wear [33]. In addition, some samples (such as Samples 3, 4 and 5) also had shallow furrows on the wear surface, which indicates that abrasive wear also occurred during the friction process. In general, the wear mechanism of the H65 copper alloy after FSP was mainly adhesive wear, accompanied by local abrasive wear. From another point of view, the change of the wear surface morphology under different process parameters is basically consistent with the change of the average friction coefficient, i.e., the smaller the average friction coefficient, the more difficult it is to wear. When the traverse speed was 200 mm/min and the rotation speed was 600 rpm, the wear surface was relatively smooth and the wear trace was the smallest, i.e., better than those of the parent metal.

## 4 Conclusions

In this paper, friction stir processing (FSP) was used to modify a larger-size surface of H65 copper alloy. The influence of the FSP process parameters on the microstructure, microhardness and wear resistance of the processed surface was analyzed. The main conclusions are as follows:

1. The greater the traverse speed, the greater the processed surface roughness. The higher the rotation speed, the lower the processed surface roughness. The grains were obviously refined after FSP and the grain size increased with the increment of the rotation speed. The cross-sectional microstructure of the processed surface can be divided into three zones: the stirring zone, the transition zone, and the parent metal zone. The grain size of the stirring zone is the smallest, which is close to the grain size of the processed surface.
2. The average microhardness of the processed surface under different process parameters was improved to varying degrees. When the traverse speed was 200 mm/min and the rotation speed was 200 rpm, the average microhardness of the processed surface was the highest (174.13 HV), i.e., 21% higher than that of the parent metal. The average microhardness decreased as the rotation speed increased under the same traverse speed. In the cross section of the processed surface, the microhardness from high to low was in the following order: stirring zone, transition zone, and parent metal zone.
3. When the traverse speed was 200 mm/min and the rotation speed was 600 rpm, the average friction coefficient of the processed surface was the lowest (0.3213), i.e., lower than that of the parent metal (0.3810). The wear mechanism of the H65 copper alloy after FSP was mainly adhesive wear, accompanied by local abrasive wear.

## Acknowledgments

This work was supported by the Open Research Project of Anhui Simulation Design and Modern Manufacture Engineering Technology Research Center (No. sgczxzd1803, sgczxzd2103, sgczxyb1807), the Natural Science Foundation of Anhui Higher Education Institutions (No. kjhs2019b15, kjhs2019b12), the Key Research and Development Project from Anhui Province of China (No. 202004a05020025) and the Special Funding for Innovative Provincial Construction Subsidy Funds (2021xzx001).

## References

[1] Davim, J.P. (ed), *Welding Technology*, ed. 1, Springer International Publishing, 2021.

[2] Mishra, R.S., De, P.S. & Kumar, N., *Friction Stir Welding and Processing*, ed. 1, Springer, 2014.

[3] Sayuti, M., Alhajji, M. & Sulaiman, S., *Mechanical Properties and Morphological Analysis of Copper Filled Aluminum Alloy Hybrid Matrix Composite*, Journal of Engineering and Technological Sciences, **52**(6), pp. 855-866, 2020.

[4] Prokhorov, V., Bagramov, R., Gerasimov, V. & Zhuravlev, V., *Copper and Its Alloys Thermal Conductivity Controlling with Diamond and Ti or Cr Addition*, Materials Today: Proceedings, **5**(12), pp. 26104-26107, 2018.

[5] Xie, Z.X., Zhang, C., Wang, R.D., Li, D., Zhang, Y.W., Li, G.S. & Lu, X.G., *Microstructure and Wear Resistance of WC/Co-based Coating on Copper by Plasma Cladding*, Journal of Materials Research and Technology, **15**, pp. 821-833, 2021.

[6] Li, Y., Cui, X.F., Jin, G., Cai, Z.B., Tan, N., Lu, B.W. & Gao, Z.H., *Interfacial Bonding Properties between Cobalt-based Plasma Cladding Layer and Substrate under Tensile Conditions*, Materials and Design, **123**, pp. 54-63, 2017.

[7] Niu, Y.R., Hu, D.Y., Ji, H., Huang, L.P. & Zheng, X.B., *Effect of Bond Coatings on Properties of Vacuum Plasma Sprayed Tungsten Coatings on Copper Alloy Substrate*, Fusion Engineering and Design, **86**(4), pp. 307-311, 2011.

[8] Morampudi, P., Venkata Ramana, V.S.N., Bhavani, K., Amrita, M., & Srinivas, V., *The Investigation of Machinability and Surface Properties of Aluminium Alloy Matrix Composites*, Journal of Engineering and Technological Sciences, **53**(4), 210412, 2021.

[9] Basuki, E.A., Adrianto, N., Triastomo, R., Korda, A.A., Achmad, T.L., Muhammad, F., & Prajitno, D.H., *Isothermal Oxidation Behavior of Ferritic Oxide Dispersion Strengthened Alloy at High Temperatures*, Journal of Engineering and Technological Sciences, **54**(2), 220210, 2022.

[10] Mishra, R.S., Ma, Z.Y. & Charit, I., *Friction Stir Processing: A Novel Technique for Fabrication of Surface Composite*, Materials Science and Engineering A, **341**(1), pp. 307-310, 2003.
[11] Kumar, R.A., Kumar, R.G.A., Ahamed, K.A., Alstyn, B.D. & Vignesh, V., *Review of Friction Stir Processing of Aluminium Alloys*, Materials Today: Proceedings, **16**, pp. 1048-1054, 2019.
[12] Reddy, G.M., Rao, A.S. & Rao, K.S., *Friction Stir Processing for Enhancement of Wear Resistance of ZM21 Magnesium Alloy*, Transactions of the Indian Institute of Metals, **66**(1), pp. 13-24, 2013.
[13] Song, W.W., Xu, X.J., Zuo, D.W. & Wang, J.L., *Study on the Corrosion of Copper Alloy by Friction Stir Surface Processing*, Anti-Corrosion Methods and Materials, **63**(3), pp. 190-195. 2016.
[14] Song, W.W., Xu, X.J., Zuo, D.W., Wang, J.L. & Wang, G., *Effect of Processing Parameters and Temperature on Sliding Wear of H62 Copper Alloy Modified by Friction Stir Surface Processing*, Materials Science, **23**(3), pp. 222-226, 2017.
[15] Heidarpour, A., Mazaheri, Y., Roknian, M. & Ghasemi, S., *Development of Cu-TiO2 Surface Nanocomposite by Friction Stir Processing: Effect of Pass Number on Microstructure, Mechanical Properties, Tribological and Corrosion Behavior*, J. Alloys Compd, **783**, pp. 886-897, 2019.
[16] Sarmadi, H., Kokabi, A.H. & Reihani, S.M.S., *Friction and Wear Performance of Copper–graphite Surface Composites Fabricated by Friction Stir Processing (FSP)*, Wear, **304**(1), pp. 1-12, 2013.
[17] Cartigueyen, S. & Mahadevan, K., *Influence of Rotational Speed on the Formation of Friction Stir Processed Zone in Pure Copper at Low-heat Input Conditions*, J Manuf Process., **18**, pp. 124-130, 2015.
[18] Moustafa, E.B., Mohamed, S.S., Abdelwanis, S., Mahmoud, T.S. & Kady, E.Y.E., *Review Multi Pass Friction Stir Processing*, American Scientific Research Journal for Engineering, Technology, and Sciences, **22**(1), pp. 98-108, 2016.
[19] Reddy, A.P., Krishna, P.V., Rao, R.N. & Murthy, N.V., *Silicon Carbide Reinforced Aluminium Metal Matrix Nano Composites – A Review*, Materials Today: Proceedings, **4**(2), pp. 3959-3971, 2017.
[20] Song, W.W., Xu, X.J., Liu, S.R., Pu, J.F. & Wang H.F., *Metallographic Organization and Tensile Properties of FSSP-modified H62 copper Alloy Surface*, Advanced Composites Letters, **29**(2), pp. 1-8, 2020,
[21] Moustafa, E.B., Melaibari, A. & Basha, M., *Wear and Microhardness Behaviors of AA7075/SiC-BN Hybrid Nanocomposite Surfaces Fabricated by Friction Stir Processing*, Ceramics International, **46**(10), pp. 16938-16943, 2020.
[22] Thankachan, T., Prakash, K.S. & Kavimani, V., *Investigating the Effects of Hybrid Reinforcement Particles on the Microstructural, Mechanical and*

*Tribological Properties of Friction Stir Processed Copper Surface Composites*, Composites Part B: Engineering, **174**, 107057, 2019.

[23] Sundaram, N.S. & Murugan, N., *Tensile Behavior of Dissimilar Friction Stir Welded Joints of Aluminium Alloys*, Materials and Design, **31**(9), pp. 4184-4193, 2010.

[24] Naldi, R., & Anawati, A., *Creep and Electrochemical Corrosion Behavior of Heattreated Mg-9Al-1Zn Alloy*, Journal of Engineering and Technological Sciences, **52**(5), pp. 609-620, 2020.

[25] Thallapalli, N., Kandi, K.K. & Batta, R., *Investigation on the Micro-structure and Mechanical Properties of Copper Based Surface Composites Fabricated by Friction Stir Processing*, Materials Today: Proceedings, **27**, pp. 1774-1779, 2020.

[26] Dinaharan, I., Sathiskumar, R. & Murugan, N., *Effect of Ceramic Particulate Type on Microstructure and Properties of Copper Matrix Composites Synthesized by Friction Stir Processing*, Journal of Materials Research and Technology, **5**(4), pp. 302-316, 2016.

[27] Abraham, S.J., Madane, S.C.R., Dinaharan, I. & Baruch, L.J., *Development of Quartz Particulate Reinforced AA6063 Aluminum Matrix Composites via Friction Stir Processing*, Journal of Asian Ceramic Societies, **4**(4), pp. 381-389, 2016.

[28] Vikas, K.S.R., Ramana, N.S.N.V., Bhavani, K., Reddy, C.K. & Srinivas, V., *Pitting Corrosion in AA7075 Friction Stir Welds on Minor Additions of Silver,* J. Eng. Technol. Sci., **53**(6), 210607, 2021.

[29] Avula, D., Kumar, R., Singh, R.K.R., Dwivedi, D. K. & Mehta, N.K., *Effect of Friction Stir Welding on Microstructural and Mechanical Properties of Copper Alloy*, World Academy of Science Engineering and Technology, **5**(2), pp. 174-182, 2011.

[30] Wang, H.F., Zuo, D.W., Liu, S.R., Pu, J.F. & Song, W.W., *Performance Analysis of Friction Stir Welded Lightweight Aluminum Alloy Sheet*, J. Eng. Technol. Sci., **52**(6), pp. 821-836, 2020.

[31] Wang, N.N., Cao, L.J. & Yin K., *Effect of Friction Stir Processing on High Temperature Friction and Wear Properties of AM60B Magnesium Alloy*, Lubrication Engineering, **45**(8), pp. 107-114, 2020. (Text in Chinese and Abstract in English)

[32] Zhang, C.L., Li, S.H., Fu, H.G. & Lin, Y.H., *Microstructure Evolution and Wear Resistance of High Silicon Bainitic Steel after Austempering*, Journal of Materials Research and Technology, **9**(3), pp. 4826-4839, 2020.

[33] Li, J.Y., Liu, T., & Guo, Y.W., *High-temperature Friction and Wear Properties of Friction Stir Procesed Aluminum Matrix Composites*, Journal of Materials Engineering, **43**(6), pp. 21-25, 2015. (Text in Chinese and Abstract in English).